Melting curve of potassium to 22 GPa

O. Narygina,* E. E. McBride, G. W. Stinton, and M. I. McMahon
SUPA, School of Physics and Astronomy, and Centre for Science at Extreme Conditions, The University of Edinburgh, Mayfield Road, Edinburgh EH9 3JZ, United Kingdom

(Received 17 January 2011; revised manuscript received 24 April 2011; published 12 August 2011)

The melting curve of potassium has been measured experimentally to 22 GPa using *in situ* X-ray diffraction and gas-membrane diamond anvil cells equipped with external resistive heating. The evolution of the melting temperature with pressure is similar to that of sodium, but it is different to that reported previously. A melting maximum is found in the stability field of the *bcc*-phase, at 5.8(5) GPa, followed by a decrease in the melting temperature down to a melting minimum at the *fcc*-host-guest (*tI*19) transition at 19(1) GPa. The *bcc*-*fcc*-liquid and *fcc*-*tI*19-liquid triple points are found to be at 466(10) K and 13.6(3) GPa and at 390(10) K and 19.0(3) GPa, respectively.

DOI: 10.1103/PhysRevB.84.054111 PACS number(s): 61.50.Ks, 64.70.dj

I. INTRODUCTION

The high-pressure behavior of the alkali metals remains a "hot topic" in both experimental and theoretical physics. Despite the apparent simplicity of these metals (a single *s* electron in the valence band), they exhibit quite peculiar properties at high pressures, such as the formation of composite and/or open-packed structures,[1] low melting temperatures,[2,3] and both a decrease in electrical conductivity and the appearance of superconductivity.[4] The pressure-induced structural behavior of the different alkali metals is broadly similar, with the main trend being transitions between simple, cubic phases (body-centered-cubic [*bcc*] and face-centered-cubic [*fcc*]) before transitions to open-packed phases with decreased structural symmetry.[1,5] Potassium (K), like the other alkali metals, crystallizes in the *bcc* structure at ambient conditions before transforming to the *fcc* phase at 11 GPa at 300 K.[6,7] Further increase of pressure leads first to a transition at 19 GPa to the incommensurate host-guest composite structure with 19.2 atoms per unit cell (hereafter referred to as *tI*19),[7] and then to the orthorhombic *oP*8 structure at 54 GPa, which is stable up to 90 GPa, where it transforms to the tetragonal *tI*4 structure, which in turn transforms to the orthorhombic *oC*16 structure at 96 GPa.[8] There is also evidence of the stabilization of the hexagonal *hP*4 structure at pressures between 25 and 35 GPa.[9] The *oP*8 and *hP*4 structures are otherwise observed only in sodium (Na), but at much higher pressures,[10,11] while the *oC*16 and *tI*4 structures are observed in both cesium (Cs) and rubidium (Rb) at high pressures.[12] The high-pressure structural behavior of K therefore has similarities to each of its group-I neighbors (Na, Rb, and Cs).

One of the common features of most of the alkali metals is complex melting behavior. The melting temperature of Na reaches a maximum of ∼1000 K at about 31 GPa in the *bcc* phase, followed by a dramatic decrease down to approximately room temperature at ∼120 GPa.[2] The appearance of one or more melting-curve maxima has also been observed in lithium (Li), Rb, and Cs,[3,13,14] but not, however, in K, at least not up to 14.5 GPa.[15] The melting curve of K has been measured to 8 GPa in a piston-cylinder apparatus.[16] Later experiments, performed up to 3 GPa using the piston piezometer method[17] and a modified piston-cylinder apparatus with a hydrostatic pressure medium,[18] have revealed that this earlier study was performed under nonhydrostatic conditions. Later, Zha and Boehler[15] extended the melting curve of K to 14.5 GPa by optical observations of a sample enclosed in a diamond anvil cell (DAC). They reported a continuous increase of the melting temperature in both the *bcc* and *fcc* phases, up to 649 K at 14.5 GPa. However, theoretical calculations of the melting temperature of K have suggested the presence of a melting maximum in the interval of 4–8 GPa.[19–21] To resolve this apparent discrepancy between experimental and theoretical results, and to extend the measurements of potassium melting curve into the incommensurate *tI*19 phase above 19 GPa, we performed an *in situ* X-ray diffraction (XRD) study of the melting curve of K at pressures up to 22 GPa using DAC techniques.

II. EXPERIMENT

High-purity (99.95+%) samples of K (Aldrich Chemical Company), along with a few small pieces of SrB_4O_7:Sm^{2+} for pressure calibration, were loaded into membrane pressure cells equipped with 300 μm-culet-size diamond anvils in a dry, oxygen-free atmosphere (<1 ppm O_2 and <1 ppm H_2O) to prevent sample oxidation. In order to avoid contamination, no pressure transmitting medium was used. While the stated purity of the sample refers to the metal content, such samples may contain nonmetallic contaminants such as oxygen. However, in a previous room-temperature study of potassium using both as-purchased and distilled samples, we observed no difference in their high-pressure behavior.[7] Diffraction patterns of the low-pressure *bcc* and *fcc* phases in the present study showed no discernible contaminant peaks, confirming that the sample was pure K.

Initial experiments conducted with rhenium (Re) gaskets showed that the K reacted with the gasket material immediately upon melting. Gold-lined Re gaskets also showed evidence of reaction. However, no reactions were observed between the liquid-K and tungsten (W) or iridium (Ir). Therefore, we employed W and composite Re-Ir gaskets in our experiments, pre-indented to 20 μm, and with an initial sample-chamber diameter of 80 to 125 μm, depending on the gasket material. For pressure measurements, the shift of the $^7D_0$–$^5F_0$ fluorescence line of SrB_4O_7:Sm^{2+} was used.[22] In

several runs, once the melting point of K was first reached, the fluorescence signal from the $SrB_4O_7:Sm^{2+}$ became very weak or disappeared entirely. In this case, the pressure was determined from the room-temperature K equation-of-state (EOS),[7] with a correction for the effects of thermal expansion, as obtained from the ambient-pressure thermal expansion,[23] and our own high-pressure, high-temperature measurements of the crystalline phases when the pressure could be directly determined from $SrB_4O_7:Sm^{2+}$. In these cases, the maximum correction that needed to be applied to the pressure determined from the room-temperature EOS was 0.5 GPa.

In order to heat the sample to the desired temperatures, we used external resistive heating K-rings (Watlow Ltd.), which allow sustained, stable, and homogeneous heating of the sample up to at least 600 K. A K-type (chromel/alumel) thermocouple, placed on the back of the diamond anvils, was used for temperature measurements; the uncertainty in temperature was estimated to be not more than 10 K. At each experimental point, the temperature before and after the X-ray exposure was the same within 2–3 K.

In situ high-pressure XRD measurements were performed on beamline ID09a at the European Synchrotron Radiation Facility (ESRF), and on beamline I15 at the Diamond Light Source (DLS). The incident X-ray wavelengths were 0.4143 Å and 0.4140 Å, and the X-ray beam sizes were approximately 10 μm and 30 μm in diameter, respectively. The XRD data were collected on a MAR555 detector (exposure time 1 s) on ID09a, and on a MAR 345 image-plate detector (exposure time 120 s) on I15. In both cases, the detectors were placed approximately 350 mm from the sample. During each X-ray exposure, the sample was oscillated $\pm 7^\circ$ around a vertical axis in order to improve the powder-averaging of the XRD patterns from polycrystalline samples, and to obtain a sufficient number of reflections to identify the crystal structure of K when the sample had annealed into a single crystal, as is discussed in the following section. The resulting two-dimensional (2D) XRD images were integrated azimuthally using Fit2D,[24] and subsequent analysis was performed either with the GSAS package,[25] or by least-squares fitting of the measured *d*-spacings.

Diffraction data were collected from ten different samples, and consistent results were obtained from all of them. In all experimental runs, the K samples were initially precompressed to a desired pressure at room temperature and then heated until melting was observed. The pressure and/or temperature of the sample were then changed to bring it back into a crystalline phase (*bcc*, *fcc*, or *tI*19 depending on the pressure). Melting was judged both from the complete disappearance of the crystalline Bragg scattering and by the simultaneous appearance of a diffuse halo of scattering from the liquid phase.

III. RESULTS

A representative set of high-pressure, high-temperature 2D XRD images, and their integrated XRD profiles, is shown in Fig. 1. They demonstrate the sharp transition from *fcc*-K to liquid-K at 18.3(3) GPa, which is induced by the small increase in temperature of only 4 K. A subsequent pressure increase of about 2 GPa at the same temperature (408[10] K) brings the sample into the stability field of the incommensurate *tI*19 phase, and results in the recrystallization of the sample. It should be noted that upon heating, K samples tend to anneal into high-quality single crystals, and, therefore, many of the high-temperature diffraction patterns collected from the solid phases during this experiment were single-crystal–like (see Fig. 1(a)). The Bragg peaks from such samples tend to rapidly saturate the detector, and hence azimuthal integration results in diffraction profiles that do not have accurate relative peak intensities. Therefore, the analysis of the integrated XRD patterns (see Fig. 1(d)) was performed using the Le Bail method. On the raw diffraction image collected from the incommensurate *tI*19-K phase at 408(10) K and 22.3(3) GPa (Fig. 1(c)), the reflections from the "host" component of the structure are sharp (Miller indices for some of which are given), while the (*hk*1) layer of "guest" reflections is extremely broad and diffuse, and appears to form an almost continuous line of diffuse intensity in the 2D images, with several weak intensity maxima. In the integrated profile, the strong (001) guest peak then appears as a broad bump (marked in Fig. 1(d) by the black arrow). The diffuse nature of the guest reflections arises from a temperature-induced reduction in the correlation length between the guest-atom chains, resulting in the broadening of the guest reflections in the *hk*-plane. We have observed such broadening previously in the composite phases of both Rb and Na.[26,27]

Integrated diffraction profiles of liquid-K collected at different pressures, with the background from the pressure cell subtracted, are shown in Fig. 2(a). In order to subtract the background, which includes both Compton scattering and thermal diffuse scattering (TDS) from the diamond anvils, we utilized the procedure described by Sanloup *et al.*[28] In this procedure, a background baseline for a diffraction profile from the liquid is obtained by the integration of a pattern collected from the solid phase immediately prior to melting, once all Bragg reflections from the solid phase have been masked. As one can see in Fig. 2(a), at pressures below 11 GPa, only the first diffraction maximum from the liquid-K is well defined; however, above 11 GPa, the much weaker second diffuse halo becomes more pronounced as pressure increases. Observation of the second diffuse halo of scattering is made more difficult by the fact that it lies at the same *d*-spacing as the TDS from the diamond anvils.

The *d*-spacing of the first diffraction maximum from the liquid is plotted as a function of pressure in Fig. 2(b) (solid circles), along with the *d*-spacing of the (110) and (111) reflections from the *bcc* (unfilled triangles) and *fcc* phases (unfilled squares), respectively. The *d*-spacing of the first diffraction maximum of the liquid at 2.2(5) GPa agrees well with the *d*-spacing of the (110) reflection from *bcc*-K, while from 5 to 15 GPa the position of the first liquid diffraction peak closely follows the *d*-spacing of the (111) *fcc*-K reflection. The kinks in the liquid data at about 5 and 15 GPa suggests changes in the compressibility of liquid-K at these pressures, the possible origin of which is discussed in the next section.

The melting curve of potassium measured to 22 GPa is shown in Fig. 3. It appears to be strikingly similar to that of Na,[2] but with the phases appearing at significantly lower pressures. All XRD patterns collected below 11(1) GPa showed the presence of single-phase *bcc*-K; and at 11–13.6 GPa (depending on the temperature), we detected the

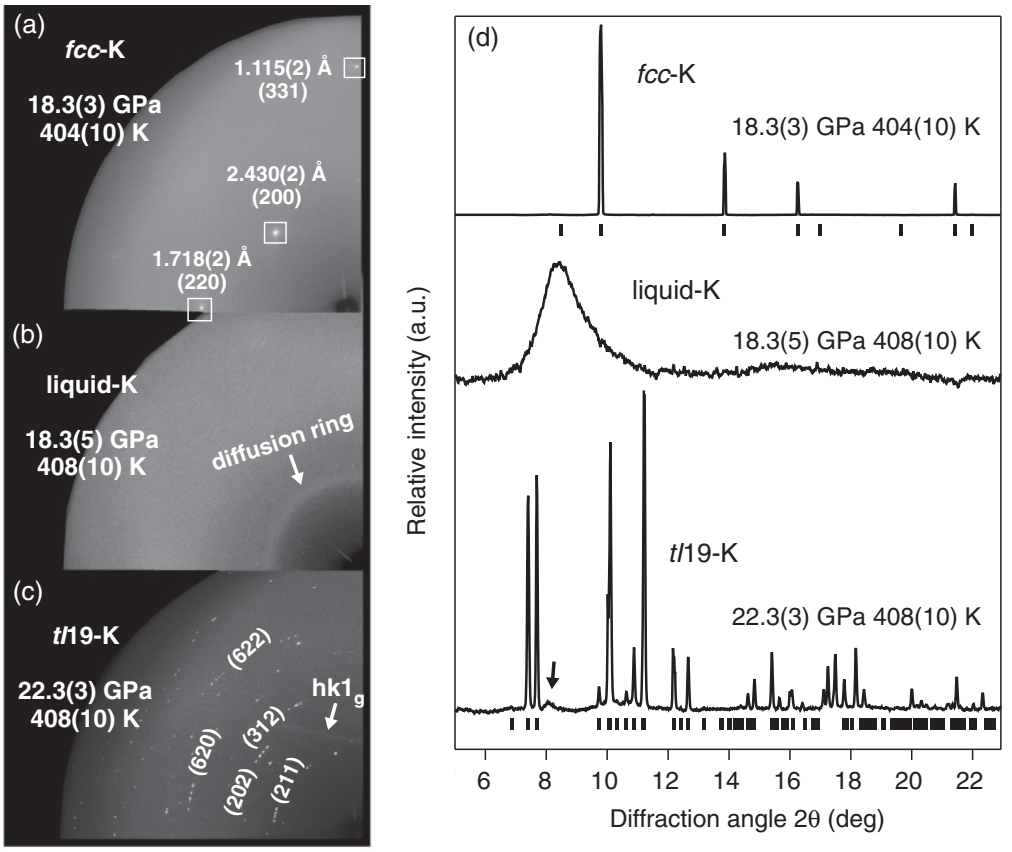

FIG. 1. (a)–(c) Representative quadrants of XRD images from the solid and liquid phases of K. Three d-spacings of *fcc*-K and Miller indices for some reflections of *tI*19-K are marked in the images (a,c), and the diffuse line of (hk1) reflections from the guest component of the *tI*19 phase is identified with the white arrow in image (c). (d) The corresponding integrated XRD profiles. The crystalline phases are indexed to the *fcc* and "host-guest" *tI*19 structures, and vertical bars show the fitted positions of the diffraction reflections of *fcc*-K ($a_{fcc} = 4.856(1)$ Å) and the "host" phase of *tI*19-K ($a_{host} = 9.769(1)$ Å, $c_{host} = 4.730(1)$ Å). The black arrow shows the position of the (001) "guest" reflection of *tI*19-K. The XRD profile of liquid-K obtained at 18.3(5) GPa and 408(10) K is plotted with the background subtracted; the background baseline was obtained by integration of the pattern collected for *fcc*-K at 404(10) K and 18.3(3) GPa after all Bragg reflections had been masked (see text for the details).

appearance of *fcc*-K. The *bcc-fcc* phase boundary was tracked using a series of small changes in pressure/temperature up to the *bcc-fcc*-liquid triple point (the area highlighted in Fig. 3), which we found to be at 466(10) K and 13.6(3) GPa. Using the ambient temperature phase transition pressure, 11 GPa[6,7] (highlighted by a star in Fig. 3), the gradient of the *bcc-fcc* phase boundary is determined to be +64(5) K/GPa. Note that the *bcc-fcc* phase boundary for K was previously reported to be almost vertical, or even to have a slightly negative gradient,[15,21] and the *bcc-fcc*-liquid triple point was previously reported to be at 566 K and 11 GPa.[15]

Within the *bcc* stability region of the phase diagram, we traversed the melting line five times, at ambient pressure, 2.2(3), 5.1(3), 7.4(3) GPa, and 11.6(3) GPa, obtaining melting temperatures of 338(2) K, 496(10) K, 536(10) K, 526(10) K, and 498(10) K, respectively. With further increases of pressure above 11.6 GPa, the melting temperature continues to fall, decreasing to 466(10) K at the *bcc-fcc*-liquid triple point at 13.6(3) GPa. At pressures above the triple point, in the *fcc* phase, the melting temperature is almost constant up to 15.6(3) GPa. Note, that we cannot rule out the presence of a second melting maximum in the *fcc*-K stability field between 13.6 and 15.6 GPa, (the presence of a second maximum was also discussed for the case of the Na melting curve,[29] and it clearly exists in the *fcc* phase of Cs[14]). However, if such a maximum exists in K, it would be very small. Above 15.6 GPa, the melting curve again changes its behavior, descending to a clear minimum at 390(10) K and 19.0(3) GPa at the *fcc-tI*19-liquid triple point. The *fcc-tI*19 phase boundary is found to be almost vertical. In the *tI*19 phase, the melting temperature increases very rapidly with pressure, changing by some 65(5) K/GPa (Fig. 3). Similar behavior is observed in Na, where the melting temperature, after passing through a deep minimum at 300 K and 118 GPa, increases again after the transition to the *tI*19 phase at 125 GPa, although the increase does not seem as rapid as in K.[10,30] This difference is most probably related to the substantial volume change of 4.1(1)% observed at the *fcc-tI*19 transition in K, which is significantly larger than the volume change of 0.5(2)% observed at the *oP*8-*tI*19 transition in Na.[7,10]

Our measured melting temperatures up to the *bcc-fcc*-liquid triple point, combined with all previous melting curve

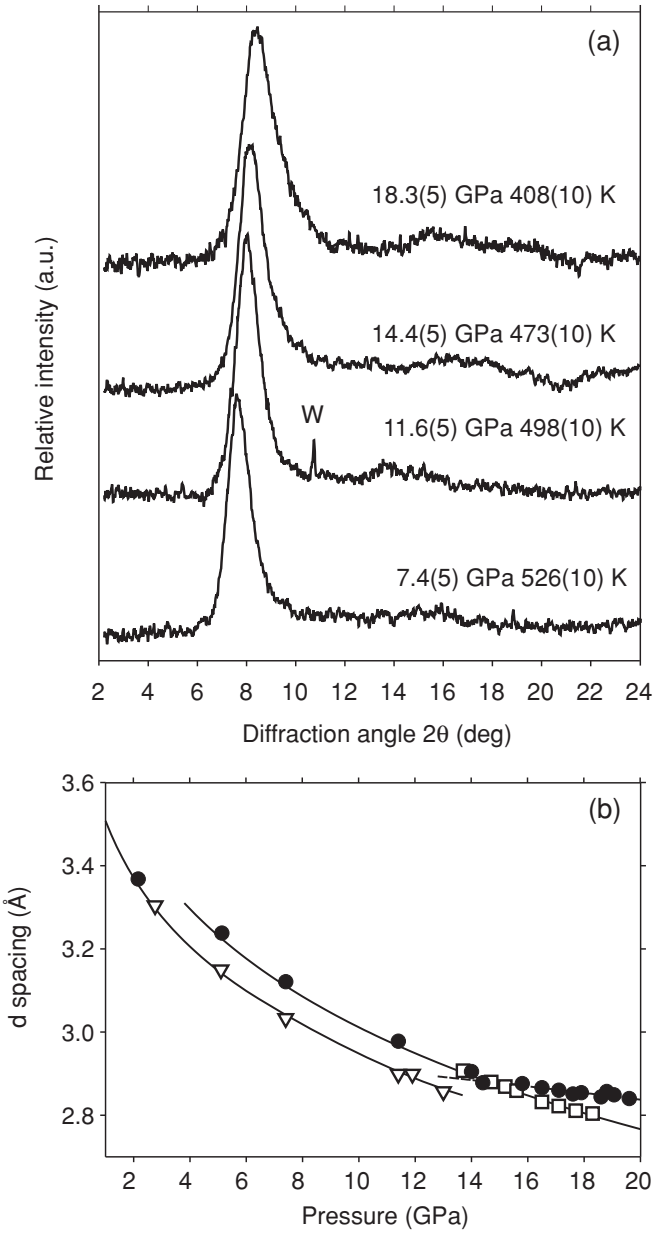

FIG. 2. (a) Integrated XRD profiles from liquid K obtained at different pressures. The background has been subtracted using the procedure described in Sanloup *et al.*[28] (see text for the details). A weak diffraction peak from the tungsten (W) gasket is marked. (b) The pressure-induced shift of the first diffraction peak from liquid-K (solid circles) and the (110) (open triangles) and (111) (open squares) diffraction peaks from *bcc*- and *fcc*-K, respectively. The lines through the data points are guides to the eye.

measurements up to 3 GPa,[16–18] suggest the presence of a melting maximum in the *bcc* phase. To locate it, we fitted these data to the Kechin equation,[31] using the following parameters: $a = 0.527(27)$, $b = 0.288(10)$, and $c = 0.045(1)$. The resulting curve (shown by the solid black line in Fig. 3) gives an excellent fit to the observed melting temperatures and suggests the maximum melting point is at 530(10) K and 5.8(5) GPa, which is in good agreement with theoretical calculations by Young and Ross[19] and Katsnelson *et al.*[21] (the dotted and dash-dotted lines in Fig. 3, respectively). Note that the existence of a melting maximum in the *bcc* phase is not dependent on the fit to the Kechin equation, as we clearly see the melting temperature of the *bcc* phase decrease between 5.1(5) GPa and 13.6(3) GPa. We use the fit simply to provide a best estimate of where the maximum is located.

As evidenced from Fig. 3, our diffraction results are in strong disagreement with the melting curve of K reported by Zha and Boehler.[15] Although some differences might arise from the use of different pressure calibrants (Zha and Boehler used ruby fluorescence, the spectrum of which gets broader and weaker at high temperatures[15]) and different sample preparation techniques (Zha and Boehler loaded their samples under mineral oil), it seems unlikely that these factors alone can explain such a significant misfit between the two data sets; the temperature difference between the two melting curves at 14.5 GPa is more than 180 K. The most likely explanation is the different way of defining the observation of melting. Zha and Boehler determined melting by visual observation of the sample, through monitoring changes in sample shape, surface texture, and reflectivity in both transmitted and reflected light. The very large differences between the melting temperatures reported in that study, and the results we report here through direct observation of melting using X-ray diffraction, strongly suggest that the changes observed by Zha and Boehler were not a result of melting.

IV. DISCUSSION

K, like Na, Rb, and Cs, is found to have a melting maximum in the *bcc* phase. The *bcc* phases of the neighboring alkaline earth elements also exhibit either a maximum, as in Ba,[32] or flat melting curves over extended pressure ranges, as in Ca and Sr.[33] The recently-observed maximum in the Li melting curve at 10 GPa may be in the *bcc* phase.[34] The appearance of a melting maximum, without the presence of a phase transition within the solid phase, is itself a manifestation of anomalous behavior of a system. According to the Clausius-Clapeyron equation, a change in the gradient of the melting slope from positive to negative suggests a change in the relative densities of the solid and liquid phases, with the liquid becoming the denser of the two at pressures above the melting maximum. This effectively means structural changes either in the liquid or solid phase, or both. In Na, it has been shown that above 30 GPa (the pressure at which the maximum melting temperature is observed), the liquid phase of Na is less compressible than the underlying *bcc* phase.[2] Molecular dynamics simulations by Hernandez and Iniguez[29] confirmed the higher compressibility of the liquid phase and suggested that while there is no dramatic change in the liquid structure on compression, there is a higher probability of *fcc*-like local order in liquid Na at higher pressures.[29] Further molecular dynamic simulations of liquid and solid Na by Raty *et al.*[35] showed changes in the second coordination shell of the liquid phase above 30 GPa. They assigned these to a change from a *bcc*-like to a *fcc*-like liquid, resulting in a negative slope of the melting curve between 30 and 65 GPa, where the solid Na itself adopts the *fcc* structure. The reason for structural and/or electronic changes to occur in a liquid state earlier than in a solid state has been discussed by several authors and is assumed to be related

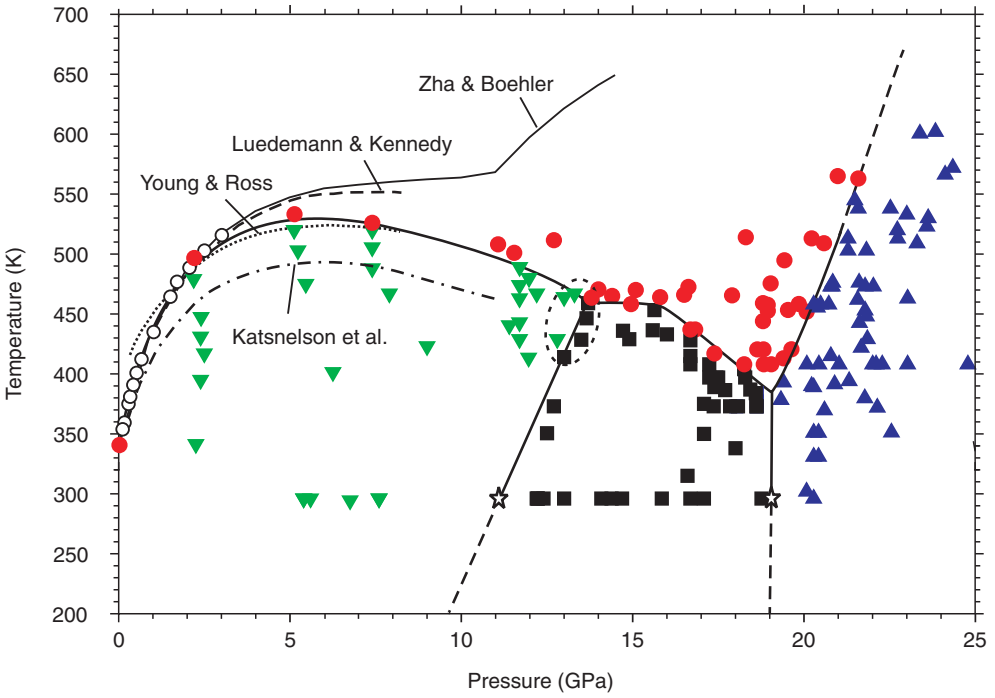

FIG. 3. (Color online) The melting curve of K measured to 22 GPa. Filled symbols represent the data from this study: downward-pointing triangles correspond to *bcc*-K, squares to *fcc*-K, upward-pointing triangles to *tI*19-K, and circles to the liquid phase. The melting temperature at ambient pressure was obtained by observation of the K sample sealed in a glass capsule. Solid and dashed lines represent the measured phase boundaries and their extrapolations, respectively. The data points marked with stars show the locations of the *bcc-fcc* and *fcc-tI*19 phase transitions at room temperature.[6,7] Open circles are data points from references 16–18. The melting curve in the pressure range from ambient up to the 13.6(3) GPa (the location of the *bcc-fcc*-liquid triple point) represents the fit of the experimental data using the Kechin equation.[31] Some previously-reported experimental and theoretically calculated melting curves of K are from references 15, 16, 19, and 21.

to the finite-temperature fluctuations in liquids, which allow changes to occur continuously over a large pressure range. In solids, they occur discretely at a definite pressure.[35,36]

Similarities in the melting curves of K and Na,[2] as well as the other similarities in the structural behavior of these two alkali elements at high compressions (discussed previously), may suggest a similar origin for the melting maximum in the stability field of *bcc*-K, namely, a decrease of compressibility of the liquid phase above 6 GPa and increasing probability of *fcc*-like local ordering. Detailed measurements of the relative compressibilities of the *bcc* and liquid phases of K along with molecular dynamics simulations are required to confirm this. However, a plot of the *d*-spacing of the first diffraction peak in liquid K implies a change in its compression behavior at about 5 GPa [Fig. 2(b)]. While at 2.2 GPa the *d*-spacing of the first diffraction peak of the liquid agrees very well with the *bcc*-K equation of state, at pressures between 5 and 14 GPa it closely follows the *fcc*-K equation of state. This suggests that the local ordering in liquid-K may change from *bcc*- to the denser *fcc*-like at about 5 GPa, i.e., almost 8 GPa below the *bcc-fcc* transition pressure in the solid phase (13.6 GPa at 455 K).

While the melting maximum in the *bcc* phase might be explained by different compressibilities of the solid and liquid phases, and an increased likelihood of *fcc*-like local ordering, this cannot explain the behavior of the K melting curve above 13.6 GPa, where the solid K itself adopts the *fcc* structure, and the melting curve remains essentially flat to 15.6 GPa before decreasing to its minimum value of 390(10) K at 19.0(3) GPa, just before the transition to *tI*19 phase (Fig. 3). Raty *et al.*[35] reported that the similar behavior of the melting curve of *fcc*-Na results from electronic and structural changes in the liquid phase that are similar to those that occur at the *fcc*-to-*cI*16 transition in the solid phase at higher pressures.[37,2] As a result, the liquid local order changes from *fcc*-like to *cI*16-like, altering the compressibility of the liquid phase. This is then reflected in the negative gradient of the melting curve of Na between 80 and 100 GPa. Above 100 GPa, where the solid transforms to the *cI*16 phase, the melting curve recovers its positive slope.[10] Since the melting behavior of *fcc*-K and *fcc*-Na is very similar, we suggest it can be explained in the same manner, namely by electronic and structural changes, which, in the case of K, result in the liquid local order changing from *fcc*-like to *tI*19-like. Figure 2(b) shows the pressure dependence of the *d*-spacing of the first diffraction peak in liquid K and the (111) diffraction peak from the *fcc*-K phase. While below 15.6 GPa both the *d*-spacing and compressibility of the peaks are the same, there is a clear change in liquid-K above that pressure, with the compressibility of the first liquid diffraction peak being somewhat less than that of the (111) diffraction peak [Fig. 2(b)]. This change in compressibility results in the negative slope of the melting curve of K between 15.6 and 19 GPa. Above 19 GPa, where the solid itself assumes the denser *tI*19 structure, the slope of the melting curve recovers a positive gradient.

However, anomalous melting behavior can also be related to structural changes in a solid. Thus, the melting of *bcc*- and *fcc*-Na can be explained in the framework of the Lindeman melting criterion, without consideration of a liquid phase. Several authors have calculated softening of the elastic moduli of solid Na above 30 GPa and a consequent decrease of the Debye temperature,[38] which, according to the Lindeman criterion, results in a negative slope of a melting curve. A strong softening of elastic moduli was also found in *fcc*-Cs,[39] the melting temperature of which also decreases with pressure.[14] The theoretical work by Katsnelson *et al.*[21] did show softening of elastic constants in both *bcc*- and *fcc*-K. Using the Lindeman criterion, they also calculated the melting curve of K, which they found to have a maximum at about 5 GPa (in good agreement with the 5.8(5) GPa presented here). However, the same calculation underestimates the melting temperature over a large pressure range (dash-dotted line in Fig. 3). The possible softening of elastic moduli in *bcc*- and *fcc*-K, and its effect on the melting curve of K, will require further experimental work.

Finally, the marked minimum of the K melting curve, just before the transition to the incommensurate *tI*19 phase, is also not unique: the melting curves of Cs, Rb, Na, and Li also reach their high-pressure minima at the transition to their high-pressure, low-symmetry phase.[2,3,13,14] In the case of Cs, superconductivity was discovered in the low-symmetry Cs-IV phase,[40] while Li becomes superconducting in the *fcc* phase, with $T_c \approx 10$ K at ∼21 GPa, which increases to 17 K at 40 GPa, i.e., the same pressure at which the melting temperature of Li reaches its minimum of 190 K, just before the transition to the *cI*16 phase.[3] Therefore, one might also expect superconducting behavior in Na, Rb, and K at pressures near the melting minimum. Indeed, theoretical work from Shi and Papaconstantopoulos[41] has predicted superconductivity in K with $T_c \approx 2$–12 K at 14 GPa (within the *fcc*-K stability field), while Sanna *et al.*[42] and Profeta *et al.*,[43] using *ab initio* electronic structure calculations, have predicted superconductivity in K with T_c increasing from 1–2 K at 21–23 GPa (within stability field of *tI*19-K) to 11 K at 29 GPa. There is to date, however, no experimental evidence of superconductivity in any phase of K, apart from a weak anomaly observed at 1.7 K at 35 GPa.[4] Further work at lower temperatures is required.

V. CONCLUSIONS

In conclusion, the melting temperature of K has been measured to 22 GPa, and it is found to be very different to that reported previously. The *bcc* phase exhibits a melting maximum like that observed previously in Na, Rb, and Cs, while the melting curve of the *fcc* phase is found to be very similar to that observed previously in Na. Using similar arguments to those put forward previously to explain the melting curve of Na, we suggest that the behavior of the K melting curve is due to structural and electronic changes in the liquid phase at about 5 and 14 GPa, which mirror those that occur in the solid phase at 13.6 and 19 GPa, respectively. However, the anomalous melting of *bcc*- and *fcc*-K may also suggest a softening of elastic moduli of these phases as pressure increases. Further work is required to understand the complex nature of dense potassium.

ACKNOWLEDGMENTS

We thank the European Synchrotron Radiation Facility (ESRF) and Diamond Light Source (DLS) for provision of synchrotron time and support. We thank A. K. Kleppe, H. Wilhelm, and A. P. Jephcoat of I15 (DLS), and S. Evans and M. Hanfland of ID09a (ESRF) for their help with the experiment. We also thank E. Gregoryanz for discussions. This work was supported by a research grant from the UK Engineering and Physical Sciences Research Council.

*Olga.Narygina@ed.ac.uk

[1] M. I. McMahon and R. J. Nelmes, Chem. Soc. Rev. **35**, 943 (2006), and references therein.

[2] E. Gregoryanz, O. Degtyareva, M. Somayazulu, R. J. Hemley, and H.-K. Mao, Phys. Rev. Lett. **94**, 185502 (2005).

[3] C. L. Guillaume, E. Gregoryanz, O. Degtyareva, M. I. McMahon, M. Hanfland, S. Evans, M. Guthrie, S. V. Sinogeikin, and H.-K. Mao, Nature Phys. **7**, 211 (2011).

[4] J. S. Schilling, High Pres. Res. **26**, 145 (2006), and references therein.

[5] K. Syassen, in *Proceedings of International School of Physics. Enrico Fermi Course CXLVII*, edited by R. J. Hemley *et al.* (IOS Press, Amsterdam, 2002), p. 251.

[6] H. Olijnyk and W. B. Holzapfel, Phys. Lett. **99**, 381 (1983).

[7] M. I. McMahon, R. J. Nelmes, U. Schwarz, and K. Syassen, Phys. Rev. B **74**, 140102 (2006).

[8] L. F. Lundegaard, M. Marqués, G. Stinton, G. J. Ackland, R. J. Nelmes, and M. I. McMahon, Phys. Rev. B **80**, 020101 (2009).

[9] M. Marqués, G. J. Ackland, L. F. Lundegaard, G. Stinton, R. J. Nelmes, M. I. McMahon, and J. Contreras-Garcia, Phys. Rev. Lett. **103**, 115501 (2009).

[10] E. Gregoryanz, L. F. Lundegaard, M. I. McMahon, C. Guillaume, R. J. Nelmes, and M. Mezouar, Science **320**, 1054 (2008).

[11] Y. Ma, M. Eremets, A. R. Oganov, Y. Xie, I. Trojan, S. Medvedev, A. O. Lyakhov, M. Valle, and V. Prakapenka, Nature **458**, 182 (2009).

[12] U. Schwarz, K. Takemura, M. Hanfland, and K. Syassen, Phys. Rev. Lett. **81**, 2711 (1998); U. Schwarz, A. Grzechnik, K. Syassen, I. Loa, and M. Hanfland, *ibid.* **83**, 4085 (1999).

[13] R. Boehler and C.-S. Zha, Physica B+C **139–140**, 233 (1986).

[14] G. C. Kennedy and P. N. La Mori, J. Geophys. Res. **67**, 851 (1962); A. Jayaraman, R. C. Newton, and J. M. McDonough, Phys. Rev. **159**, 527 (1967); I. N. Makarenko, V. A. Ivanov, and S. M. Stishov, JETP Lett. **18**, 187 (1973).

[15] C.-S. Zha and R. Boehler, Phys. Rev. B **31**, 3199 (1985).

[16] H. D. Luedemann and G. C. Kennedy, J. Geophys. Res. **73**, 2795 (1968).

[17]I. N. Makarenko, A. N. Nikolaenko, and S. M. Stishov, in *High Pressure Science and Technology, Sixth AIRAPT Conference (1977) 347*, edited by K. D. Timmerhaus and M. C. Barber (Plenum, New York, 1979).
[18]R. Boehler, Phys. Rev. B **27**, 6754 (1983).
[19]D. A. Young and M. Ross, Phys. Rev. B **29**, 682 (1984).
[20]N. Dass, Phys. Rev. B **52**, 3023 (1995).
[21]M. I. Katsnelson, G. V. Sinko, N. A. Smirnov, A. V. Trefilov, and K. Yu. Khromov, Phys. Rev. B **61**, 14420 (2000).
[22]A. Lacam and C. Chateau, J. Appl. Phys. **66**, 366 (1989).
[23]D. R. Schouten and C. A. Swenson, Phys. Rev. B **10**, 2175 (1974).
[24]P. Hammersley, *Reference Manual V3.1 ESRF Internal Report ESRF98HA01T*, ESRF, Grenoble (1998).
[25]C. Larson and R. B. Von Dreele, Los Alamos National Laboratory Report LAUR 86 (2004), p. 748.
[26]M. I. McMahon, S. Rekhi, and R. J. Nelmes, Phys. Rev. Lett. **87**, 055501 (2001).
[27]L. F. Lundegaard, E. Gregoryanz, M. I. McMahon, C. Guillaume, I. Loa, and R. J. Nelmes, Phys. Rev. B **79**, 064105 (2009).
[28]C. Sanloup, E. Gregoryanz, O. Degtyareva, and M. Hanfland, Phys. Rev. Lett. **100**, 075701 (2008), and reference therein.
[29]E. R. Hernandez and J. Iniguez, Phys. Rev. Lett. **98**, 055501 (2007).
[30]M. Marqués, M. Santoro, C. L. Guillaume, F. Gorelli, J. Contreras-García, R. Howie, A. F. Goncharov, and E. Gregoryanz, Phys. Rev. B **83**, 184106 (2011).
[31]V. V. Kechin, J. Phys. Condens. Matter **7**, 531 (1995); Phys. Rev. B **65**, 052102 (2001).
[32]M. Winzenick and W. B. Holzapfel, Phys. Rev. B **55**, 101 (1997).
[33]D. Errandonea, R. Boehler, and M. Ross, Phys. Rev. B **65**, 012108 (2001).
[34]A. Lazicki, Y. Fei, and R. Hemley, Solid State Commun. **150**, 625 (2010).
[35]J.-Y. Raty, E. Schwegler, and S. A. Bonev, Nature **449**, 448 (2007).
[36]S. A. Bonev, E. Schwegler, T. Ogitsu, and G. Galli, Nature **431**, 669 (2004).
[37]V. F. Degtyareva, High Press. Res. **23,** 253 (2003), and references therein.
[38]M. Martinez-Canales and A. Bergara, J. Phys. Chem. Solids **69**, 2151 (2008); L. Koči, R. Ahuja, L. Vitos, and U. Pinsook, Phys. Rev. B **77**, 132101 (2008); S. V. Lepeshkin, M. V. Magnitskaya, and E. G. Maksimov, JETP Lett. **89**, 688 (2009).
[39]V. G. Vaks, M. I. Katsnelson, A. I. Likhtenstein, G. V. Peschanskikh, and A. V. Trefilov, J. Phys. Condens. Matter **3**, 1409 (1991).
[40]J. Wittig, Phys. Rev. Lett. **24**, 812 (1970); in *Superconductivity in d- and f-Band Metals*, edited by W. Buckel and W. Weber (Kernforschungszentrum, Karlsruhe, 1982), p. 321.
[41]L. Shi and D. A. Papaconstantopoulos, Phys. Rev. B **73**, 184516 (2006).
[42]A. Sanna, C. Franchini, A. Floris, G. Profeta, N. N. Lathiotakis, M. Lüders, M. A. L. Marques, E. K. U. Gross, A. Continenza, and S. Massidda, Phys. Rev. B **73**, 144512 (2006).
[43]G. Profeta, C. Franchini, N. N. Lathiotakis, A. Floris, A. Sanna, M. A. L. Marques, M. Lüders, S. Massidda, E. K. U. Gross, and A. Continenza, Phys. Rev. Lett. **96**, 047003 (2006).